

Article

Simulation and Verification of Involute Spline Tooth Surface Wear before and after Carburizing Based on Energy Dissipation Method

Xiangzhen Xue ^{1,*}, Jian Liu ¹, Jipeng Jia ¹, Siwei Yang ² and Yifan Li ¹¹ Mechanical and Electrical Engineering, Shaanxi University of Science and Technology, Xi'an 710021, China² Science and Technology on Helicopter Transmission Laboratory, Zhuzhou 412002, China

* Correspondence: xuexiangzhen@sust.edu.cn

Abstract: This work studies the tooth surface wear of floating involute spline couplings. Based on the energy dissipation method, this study takes the floating involute spline couplings as the research object, divides the whole wear cycle into three wear stages and analyzes its wear mechanism, and proposes a wear prediction model suitable for floating involute spline couplings. By using Abaqus, the simulation of the involute spline couplings before and after carburizing was carried out when the floating distance was 0 mm, 0.3 mm and 0.6 mm, respectively. The wear depth of each tooth was compared and analyzed, and the axial and radial distributions of the wear on the tooth surface of the involute spline couplings were explored. Finally, the floating involute spline couplings test bench was used to verify the spline wear before and after carburizing. The results show that with the increase in floating distance, the wear of the tooth surface also increases, and the upper edge of the tooth surface is seriously worn. Through the comparative analysis of the spline tooth surface wear before and after carburizing treatment, it can be seen that carburizing treatment can effectively reduce the wear degree of the spline couplings tooth surface and improve the service life of the spline couplings, but at a high floating distance, carburizing treatment has no significant effect on improving the performance of the tooth surface.



Citation: Xue, X.; Liu, J.; Jia, J.; Yang, S.; Li, Y. Simulation and Verification of Involute Spline Tooth Surface Wear before and after Carburizing Based on Energy Dissipation Method. *Machines* **2023**, *11*, 78. <https://doi.org/10.3390/machines11010078>

Academic Editors: Thomas Hagemann and Hubert Schwarze

Received: 3 December 2022

Revised: 6 January 2023

Accepted: 6 January 2023

Published: 8 January 2023



Copyright: © 2023 by the authors. Licensee MDPI, Basel, Switzerland. This article is an open access article distributed under the terms and conditions of the Creative Commons Attribution (CC BY) license (<https://creativecommons.org/licenses/by/4.0/>).

Keywords: involute spline; floating distance; finite element model; wear depth; carburizing treatment

1. Introduction

The reason involute spline couplings are widely used in aviation drive systems is that the connection of the spline couplings can meet the connection requirements of larger torque and higher speed; second, its assembly mode is a coaxial connection to ensure good guidance and neutrality between the shaft parts and the main shaft of the power system [1]. There are gaps between floating spline tooth surfaces, between internal and external tooth tops, and between adjacent tooth roots; it is required to select the tooth profile corresponding to the backlash, which is different from the centering method of the fixed involute spline. This kind of non-centering connection allows a certain axis displacement between the spline shaft and the spline sleeve during operation to compensate for the design, manufacturing, processing, and assembly errors [2]. When the spline coupling transmits torque, there is slight relative movement between the internal and external splines due to the existence of backlash. On the other hand, the axial floating of the spline couplings is caused by the existence of axial force or the change in the external load. Under the combined effect of these two factors, the tooth surface wear failure of the aviation gradually floating open spline couplings is extremely serious. Because the axial floating distance is not parallel to the axis, the lubrication is not sufficient, and the wear particles easily accumulate, causing serious wear on the tooth surface. The problem of premature failure of components caused by excessive wear of floating splines has occurred many

times in the aviation drive system, which is one of the key technologies restricting the improvement of the life and reliability of drive components.

Xue et al. [3,4] studied the wear of aviation floating involute spline couplings under different tooth surface wear factors, loads, and operating cycles by using the finite element method and designed a planar spline coupling structure that can simulate the floating involute spline couplings to verify theoretical research. Tang [5] studied the influence of different lubrication methods and surface treatment on the wear of the spline couplings of the helicopter reducer through finite element simulation and carried out simulation analysis. The conclusion is that the stress distribution of the spline tooth surface is relatively uniform under different friction factors. With the increase in dynamic friction coefficient, the friction between spline contact surfaces increases, the average contact stress of tooth surface increases with the increase in the friction coefficient, and the relative sliding speed of spline tooth surface decreases with the increase in the friction coefficient.

Xu et al. [6,7] verified the accuracy of the optimized Archard wear calculation model by combining pin on disk wear test with ANSYS and then studied the influence of backlash, including angle and modification amount on tooth surface wear. They used mathematical models to fit the three to obtain the best involute spline couplings parameters to achieve the role of wear reduction and wear resistance. As for the research on the load distribution on the tooth surface of the spline couplings, Tan et al. [8,9] researched the load distribution of the involute spline couplings in the case of misalignment. The research shows that the radial misalignment of the involute spline couplings is more serious than the axial misalignment, and the radial misalignment plays a major role in the case of the combination of the two misalignments. Wei et al. [10,11] established the finite element model of the involute spline couplings of the shield shaft and studied the stress distribution on the tooth surface of the spline couplings in the working process; the research showed that when the spline couplings transmit the load, there is stress concentration on the tooth surface along the axial and radial directions, the spline teeth are modified along the tooth profile and tooth direction, respectively, and the involute spline couplings after the modification are simulated in a limited way. The research shows that the stress concentration on the tooth surface of the involute spline couplings after the modification is significantly improved, and the reliability of the involute spline couplings of the shield shaft is improved.

Many scholars have also carried out research on this topic. Ratsimba et al. [12] proposed a prediction method for fretting wear of spline couplings based on the Archard model. McColl [13] proposed a finite element method to calculate fretting wear based on the modified Archard equation, but it simulates the wear process of a pin disk structure. At present, when calculating the tooth surface wear of the involute spline couplings, the Archard wear formula is often used, and the model in the research content has also been simplified. The existing Archard wear formula is not suitable for calculating the wear depth of the aviation floating involute spline couplings. Baker et al. [14] studied the working process of the straight tooth spline couplings, established the finite element model of the straight tooth spline couplings, analyzed the simulation results of the spline couplings under the combined working conditions of axial load, torque, and bending moment, and studied and analyzed the distribution of contact stress on the tooth surface. Leen et al. [15–17] took helical spline couplings as the research object, explored the influence of axial load and torque on the distribution of tooth surface contact stress of helical spline couplings, and carried out relevant research on the influence of different spline tooth modifications on tooth surface contact stress distribution under fixed axial load. Medina et al. [18–20] studied the influence of the main parameters of the spline couplings on contact stress and slip distance of the spline couplings' tooth surface. At the same time, the changes in the contact stress and slip distance of the spline tooth surface when the external torque and axis offset of the spline couplings' change are studied. Hong et al. [21,22] also took helical spline couplings as the research object, analyzing the change in tooth surface contact stress when helical spline couplings with different angles are operating to obtain the helical tooth angle with the best distribution of tooth surface contact stress. Ding et al. [23,24] obtained

the wear factor of material through a wear test, deduced the fretting wear mechanism of spline couplings, simulated the spline couplings under different working conditions, and verified the fretting wear mechanism of the spline couplings through simulation. Compared with the Archard model, the energy dissipation method has the advantage that the wear coefficient will not change due to the change in displacement amplitude. A large number of scholars have made a series of related studies using the energy dissipation method [25]. Matveevsky et al. [26] proposed to explore that the fretting wear amount of Hertz point contact and line contact under oil lubrication is related to the friction energy loss per unit area, that is, the friction power intensity. Fouvry et al. [27,28] put forward the energy wear coefficient, which can link the change in wear amount with the additional energy loss caused during fretting wear. Zhang et al. [29] proposed a finite element method based on the energy method, which can compare the differences between contact objects under the same boundary, normal phase load, and displacement conditions. Zhang et al. [30] proposed the calculation method of dynamic response and vibration contact energy dissipation of damped free vibration and simple harmonic forced vibration and carried out an analysis of their mechanical properties. Yang et al. [31] put forward an energy dissipation estimation method in the process of metal high cycle fatigue based on infrared thermal imaging, introduced natural convection and radiation thermal resistance according to heat transfer theory, and verified the correctness and accuracy of the method through numerical simulation and experiments. Therefore, considering the complexity of the working process of the floating involute spline couplings, to make the calculation result of the wear depth more accurate, this paper also uses the energy dissipation method to calculate the wear depth of the tooth surface. Therefore, the wear process is regarded as a system from the perspective of energy, and the wear process of materials is regarded as an energy transformation [32].

Based on the energy dissipation method and the actual working conditions of the aviation floating involute spline couplings, this article proposed a wear calculation model for the aviation floating involute spline couplings with axial floating distance. The distribution law of tooth surface wear of involute spline couplings before and after carburizing treatment was investigated. The axial floating distances were set to be 0 mm, 0.3 mm, and 0.6 mm, respectively. The contact stress and relative slip rate between teeth under these three working conditions were analyzed in Abaqus software, and the distribution law of wear depth of spline tooth surface along the axial and radial direction was studied based on the simulation results. Finally, the simulation results were verified through experiments, it provides a theoretical basis for the design and maintenance of aviation involute spline couplings.

Different from other studies, this study divided one wear cycle of floating involute spline couplings into three wear stages, analyzed the main wear forms of the three wear stages, respectively, and derived the wear depth calculation model suitable for floating involute spline couplings, which provides an important mathematical basis for the subsequent study of floating involute spline to establish a dynamic model. In addition, this paper also carburized the spline couplings, which is relatively rare in the study of spline friction and wear properties, providing a necessary theoretical idea for the aviation manufacturing industry to design and process high-performance and efficient spline couplings.

2. Wear Prediction Model of Floating Spline Couplings

2.1. Wear Mechanism Analysis of Floating Spline in the Working Process

According to the wear theory and process analysis [33], because of the actual working process of the floating involute spline couplings, the wear stages are divided into stage I, stage II, and stage III, respectively, corresponding to the low wear stage, the wear conversion stage, and the severe wear stage.

In stage I, when the internal and external splines just started to make contact, with the change in temperature, the lubricating oil in the contact area was forced out, resulting in poor lubrication conditions. In addition, there was a floating distance at the end of the

transmission shaft, which caused the internal and external splines to have a sliding distance. At this stage, the spline wear was mainly adhesive, accompanied by slight abrasive wear.

In stage II, due to the continuous accumulation of wear particles on the spline contact surface in stage I and the increase in temperature after working for a while, the adhesion effect between metals occurs, and the adhesion node formed by this effect shears and breaks with the relative sliding of the friction pair surface, resulting in a large amount of adhesive wear on the surface and subsurface of the motion pair and metal migration and the separation of metal particles. These separated metal particles act as wear particles, promoting and accelerating the appearance of more furrows on the spline couplings contact surface at this stage, so the wear of wear particles is aggravated. Therefore, at this stage, the spline wear is mainly (collectively called) abrasive wear and adhesive wear.

In stage III, with the increase in the spline working time and wear in stages I and II, the working stability of spline couplings and the performance of the tooth surface decrease significantly. With the increase in the floating distance, the wear of the tooth surface becomes more serious. At this time, the worn form of the tooth surface is mainly adhesive wear with oxidation wear.

To sum up, the analysis of the wear stage of the floating involute spline couplings is shown in Figure 1, where $0 \sim t_1$ is the wear of stage I, and the main wear form is adhesive wear; $t_1 \sim t_2$ is the wear of stage II, and the main wear forms are adhesive wear and abrasive wear; and $t_2 \sim t_3$ is the wear of stage III, and the main wear form is adhesive wear.

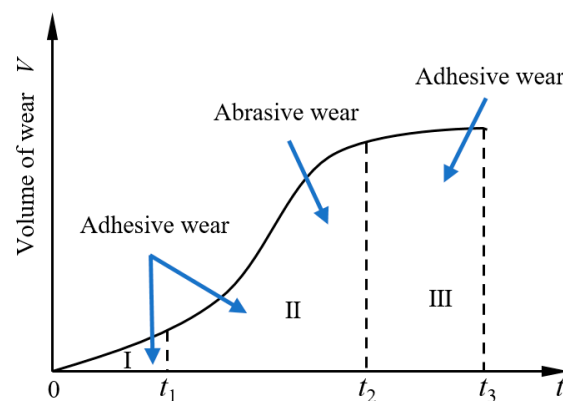


Figure 1. Analysis of three wear stages of floating involute spline couplings.

2.2. Calculation Model of Wear Depth of Floating Involute Spline

In the existing research on the calculation of tooth surface wear of floating involute spline couplings, the Archard wear equation is usually used, and the Archard model is often applied to the case of large relative slips between contact planes. However, due to the existence of the axial floating distance, the meshing degree of the tooth surface of the internal and external spline couplings is also constantly changing. The Archard model cannot accurately analyze the surface contact under this condition and cannot accurately calculate the adhesive wear and abrasive wear between the internal and external splines of the floating involute. The energy dissipation method is based on the relationship between the wear amount and the energy loss in the wear process, which is more suitable for the wear process of floating involute spline couplings.

In the energy dissipation equation, it is assumed that the relationship between the wear amount and the energy lost in the friction process is linear. The relationship between the wear volume V and the dissipated energy E_i in a cycle is:

$$V = \alpha \sum_{i=1}^N E_i \quad (1)$$

Among them, α is the energy wear coefficient of the interaction studied under a given sliding amplitude, which can be deduced from the Coulomb formula as $\alpha = k/\mu$, μ is the

friction coefficient of the contact surface, k is pressure coefficient on the contact surface of spline couplings and N is the total number of cycles included in the spline couplings wear process. The relationship between the auxiliary loss volume V of the floating involute spline is shown in Equation (2).

$$V = V_I + V_{II} + V_{III} \quad (2)$$

where 1 is the wear amount of stage I in the wear life cycle of spline couplings; 2 is the wear amount of stage II in the wear life cycle of spline couplings; and 3 is the wear amount of stage III in the wear life cycle of spline couplings.

In stage I, the worn form is mainly adhesive wear. Based on the energy dissipation method, set the sliding distance increment of ds and take differential transformation for a linear contact area with a small area of dx :

$$\frac{V_I}{dx} = \alpha \cdot \frac{Q}{dx} \cdot ds \quad (3)$$

where Q is the tangential force generated in the process of friction and wear. In the initial wear stage, the tooth surface is relatively flat and Q is relatively evenly distributed, so the shear stress at this stage is approximately regarded as a fixed value where the shear stress $q = Q/dx$ is:

$$dh_I = \alpha \cdot q \cdot ds \quad (4)$$

$$\frac{dh_I}{dt} = \alpha \cdot q \cdot \frac{ds}{dt} \quad (5)$$

$$\dot{h}_I = \alpha \cdot q \cdot v_{slip} \quad (6)$$

where \dot{h}_I is the normal wear speed of stage I in the wear life cycle of spline couplings; v_{slip} is the relative slip rate of the contact area. The time integration on both sides of the equation is as follows:

$$h_I = \int_0^{t_1} \dot{h}_I dt = \int_0^{t_1} \alpha \cdot q \cdot v_{slip} \cdot dt \quad (7)$$

Therefore, the calculation formula of stage I in the wear calculation model of floating involute spline couplings is as shown in Equation (7).

In stage II, the wear forms are mainly abrasive wear and adhesive wear. According to reference [33], this paper mainly considers the influence of slip rate and normal load and calculates the wear depth of abrasive wear and adhesive wear in the stage II, and then calculates the general formula of wear depth in stage II. Since the wear calculation formula of adhesive wear has been derived in stage I, the derivation will not be repeated here. Here, it is only necessary to deduce the formula for calculating the wear depth of stage II and then calculate the formula for calculating the wear depth of stage II.

Define the sliding distance micro increment ds ; Q_i is the tangential force generated in the process of friction and wear. In stage II, wear particles are produced due to abrasive wear, which leads to flat contact surfaces and different sizes of wear particles. Therefore, the shear stress is regarded as a variable. At this time, the shear stress $q_i = Q_i/dx$ is a differential transformation of a linear contact area with a small area of dx :

$$\frac{V_{II}''}{dx} = \alpha \cdot \frac{Q_i}{dx} \cdot ds \quad (8)$$

$$dh_{II}'' = \alpha \cdot q_i \cdot ds \quad (9)$$

$$\frac{dh_{II}''}{dt} = \alpha \cdot q_i \cdot \frac{ds}{dt} \quad (10)$$

$$\dot{h}_{II}'' = \alpha \cdot q_i \cdot v_{slip} \quad (11)$$

where $\dot{h}_{II''}$ is the normal wear speed under abrasive wear in stage II of the spline coupling wear's life cycle, and v_{slip} is the relative slip rate of the contact area. The time integration on both sides of the equation is as follows:

$$h_{II''} = \alpha \int_{t_1}^{t_2} q_i \cdot v_{slip} dt \quad (12)$$

That is to say, the calculation of the wear depth of abrasive particles applicable to floating involute spline couplings obtained by the energy dissipation method is shown in Equation (12). In combination with Equation (7) for calculating the adhesive wear depth, the formula for calculating the wear depth of floating involute spline couplings in stage II is shown in Equation (13):

$$h_{II} = \alpha \int_{t_1}^{t_2} q \cdot v_{slip} \cdot dt + \alpha \int_{t_1}^{t_2} q_i \cdot v_{slip} \cdot dt \quad (13)$$

In stage III, the worn form of the spline couplings tooth surface is mainly adhesive wear, and the wear depth at this time is calculated as shown in Equation (14).

$$h_{III} = \int_{t_2}^{t_3} \dot{h}_{III} \cdot dt = \alpha \int_{t_2}^{t_3} q_i \cdot v_{slip} dt \quad (14)$$

In conclusion, the formula for calculating the wear depth of floating involute spline couplings is finally determined as shown in Equations (16) and (17):

$$h = h_I + h_{II} + h_{III} \quad (15)$$

$$h = \alpha \int_0^{t_1} q \cdot v_{slip} \cdot dt + \alpha \int_{t_1}^{t_2} q \cdot v_{slip} \cdot dt + \alpha \int_{t_1}^{t_2} q_i \cdot v_{slip} dt + \alpha \int_{t_2}^{t_3} q_i \cdot v_{slip} dt \quad (16)$$

$$h = \alpha \int_0^{t_2} q \cdot v_{slip} \cdot dt + \alpha \int_{t_1}^{t_3} q_i \cdot v_{slip} dt \quad (17)$$

where $0 \sim t_1$ is the wear time of stage I, $t_1 \sim t_2$ is the wear time of stage II, and $t_2 \sim t_3$ is the wear time of stage III.

3. Simulation and Analysis of Wear Depth Distribution of Floating Spline Couplings after Different Surface Hardening Treatments

The optimized formula for calculating the wear depth of floating involute spline couplings of Equation (17) obtained in Section 2.2 is combined with the finite element simulation calculation, the aviation floating involute spline couplings under actual working conditions is modeled and calculated in Abaqus software, and the simulation results of the contact stress and relative slip rate of the spline couplings tooth surface are obtained. The contact stress and relative slip rate at the node of the spline couplings tooth surface obtained by simulation vary with the time increment step, which is brought into the optimized wear depth calculation Equation (17) to calculate the wear depth value of a node of the spline couplings tooth surface.

3.1. Establishment of Finite Element Model of Floating Spline Couplings

According to the involute spline couplings parameters in Table 1, the finite element solid model of a floating aviation involute spline couplings will be established. The hexahedral finite element mesh has the advantages of high calculation accuracy and good convergence. Therefore, the finite element mesh is discretized into a hexahedral mesh, and the element type of the mesh is defined as C3D8R. The fully integrated element is often shear self-locking under the action of load, and because it is a rigid element, it cannot ensure the accuracy of the calculation. When the reduced integral element is used for analysis, even if the mesh is twisted, the calculation accuracy will not be greatly affected, and it will

not be self-locking under the effect of bending load. Therefore, to reduce the calculation time and improve the calculation accuracy, all hexahedral finite element meshes in the external spline and internal spline models in this paper use the linear reduced integral element C3D8R. In this study, the penalty contact method of contact algorithm is used to define the tangential behavior and normal behavior of two contact surfaces. The tangential behavior is penalty friction, and the normal behavior is hard contact. The different working conditions of the internal and external splines are set in the assembly body. By adjusting the linear distance between the two coupled RP points, the floating amount can be changed so that one RP point rotates around the other, which is to change the angular misalignment. The physical parameter settings of materials in the model are shown in Table 2. Finally, the finite element model of the floating aviation involute spline couplings established in ABAQUS is shown in Figure 2 below.

Table 1. Involute spline coupling parameters.

Item	Parameter	Item	Parameter
Number of teeth z	12	Contact Length/mm	10
Modulus m /mm	1.25	Torque T /N · m	50
Speed N /r/min	900	Outer spline inner hole diameter D_b /mm	8
Internal spline shaft diameter D_0 /mm	25		

Table 2. The physical parameter settings of materials.

Item	Poisson's Ratio	Friction Factor μ	Elastic Modulus E /GPa
1	0.25	0.1	196
2	0.3	0.2	210

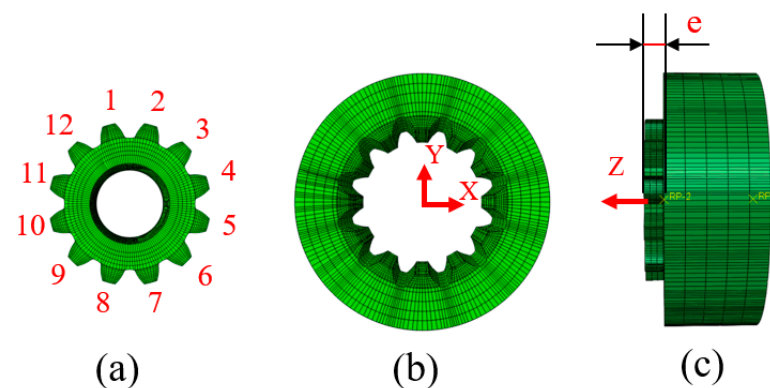


Figure 2. Finite element model of spline couplings. (a) External spline; (b) internal spline; (c) spline coupling engagement diagram.

Among them, the parameters in line 1 are the physical parameters without carburizing treatment; the parameters in line 2 are physical parameters after carburizing treatment.

3.2. Working Conditions

The finite element model of the floating involute spline couplings is constrained according to the actual installation mode of the floating involute spline couplings. In the finite element analysis software, the influence of the floating distance factor is considered. The axial floating distance of the parallel misalignment of the spline couplings and whether the tooth surface is carburized and hardened are taken as variables. Specific parameter settings are shown in Table 3. In the simulation process, the internal spline degrees of freedom only release the rotation of the Z axis, while the external spline degrees of

freedom not only release the rotation of the Z axis but also change the value of the floating distance e along the Z axis, as shown in Figure 2c. Then, the wear of the spline couplings under different working conditions is simulated, and the wear depth values under various working conditions obtained from the simulation are analyzed. It should be noted that only one simulation is conducted for each working condition in this study. Since each simulation is unrepeatable, the calculated wear depth is also unique.

Table 3. Working condition parameters.

Serial No	Tooth Surface Condition	Floating Distance e
1	Unhardened	0 mm
2		0.3 mm
3		0.6 mm
4	After hardening	0 mm
5		0.3 mm
6		0.6 mm

4. Wear Analysis of 32Cr3MoVA Involute Spline Tooth Surface without Carburizing Treatment

As an example of splines other than those in this section, the axial and radial wear distribution law of the tooth surface of the spline couplings without carburizing treatment and the wear distribution law of each tooth surface is analyzed, respectively, when the floating distance is 0 mm, 0.3 mm, and 0.6 mm. To further characterize the distribution of the tooth surface in the three wear stages, t_1 is selected from stage I of the wear cycle; t_2 , t_3 , and t_4 are selected from stage II of the wear cycle; and t_5 is selected from the III of the wear cycle, and the wear distribution law of the tooth surface at these five times is analyzed (the simulation is only conducted once for each working condition, and the simulation process is unique, so the wear depth value is also non-repeatable).

4.1. Floating Distance Is 0 mm

When the floating distance is 0 mm, simulate the actual spline couplings and obtain the distribution curve of the axial and radial wear depth of a tooth surface of the involute spline, as shown in Figures 3 and 4. When the floating distance is 0 mm, the tolerance grade of the model is 6, and the backlash is randomly distributed, so there is a certain difference in the distribution of wear depth among the teeth.

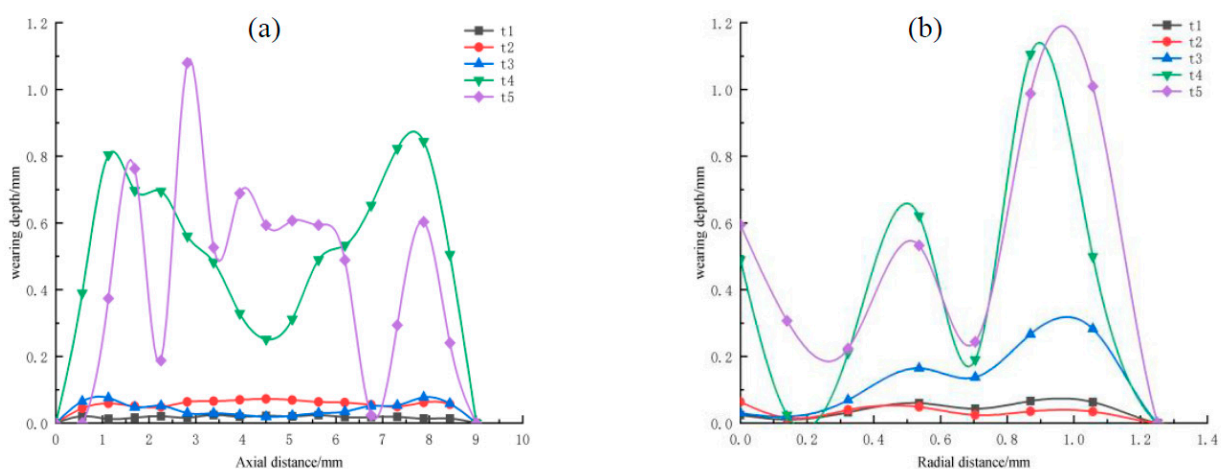


Figure 3. Wear distribution diagram of the tooth surface of the external spline without carburizing treatment when the floating distance is 0 mm. (a) Wear depth distribution curve of the external spline in the axial direction; (b) distribution curve of wear depth of external spline in the radial direction.

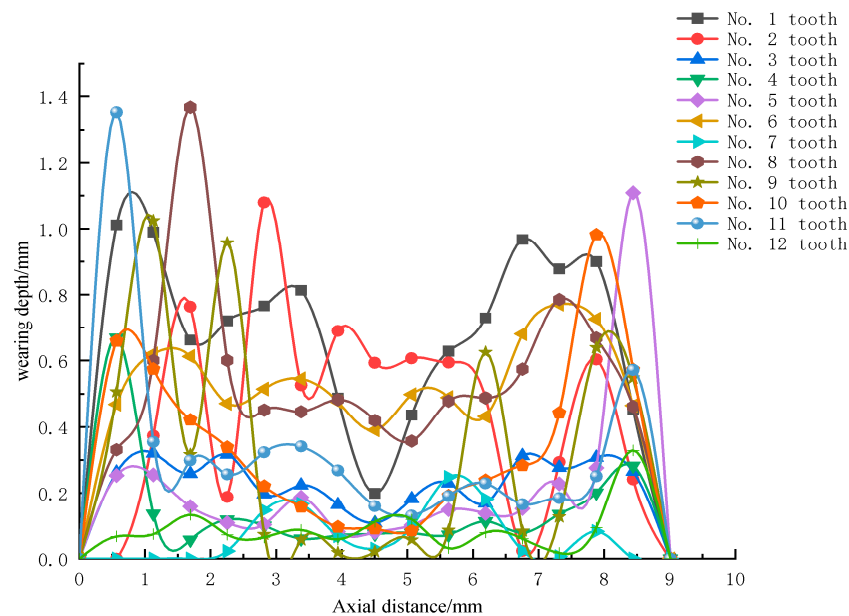


Figure 4. Distribution curve of wear depth of each tooth surface of external spline without carburizing treatment when the floating distance is 0 mm.

According to Figure 3a,b, the maximum wear depth is at 1 mm and 8 mm along the axial direction, the minimum is at 2 mm and 7 mm, the maximum is from 0.8 mm to 1.0 mm along the radial direction, and the minimum is at 0.2 mm. Regardless of the axial or radial position, the maximum wear depth is located at both ends of the tooth surface, and the wear depth at the middle part is the smallest. The fretting increases with time, leading to an increase in wear depth. In the figure, the fretting wear degree at t_1 and t_2 is smaller. This may be because the fretting wear degree is lighter at the initial stage of fretting due to good lubrication and the existence of oxide film. The fretting wear degree at t_3 and t_4 stages start to increase, which may be due to the extrusion of the lubricating fluid, the rupture of the oxide film, and the generation of a large number of metal particles between the spline couplings contact surfaces. These particles act as abrasive particles after oxidation, which aggravates the fretting wear. The fretting wear degree decreases at the t_5 stage; this may be due to the formation of a three-body bed of wear particles generated between the contact surfaces of spline couplings, which plays a role in lubrication and adjustment. Therefore, the fretting wear degree increases.

In Figure 4, when the axial floating distance is 0 mm, the wear depth of each tooth is different, which may be due to the influence of tooth clearance and mass eccentricity. In addition, the wear of each tooth at 0–2 mm and 8–9 mm at both ends is relatively large. This is because the spline couplings repeatedly make contact with the edge of the tooth when it is just in contact during the working process, resulting in serious wear at the edge of the tooth.

4.2. Floating Distance Is 0.3 mm

When the floating distance is 0.3 mm, the actual spline couplings are simulated, the wear depth of the tooth surface is calculated and analyzed, and the axial and radial wear depth distribution curve of a tooth surface of the involute external spline is obtained, as shown in Figures 5 and 6.

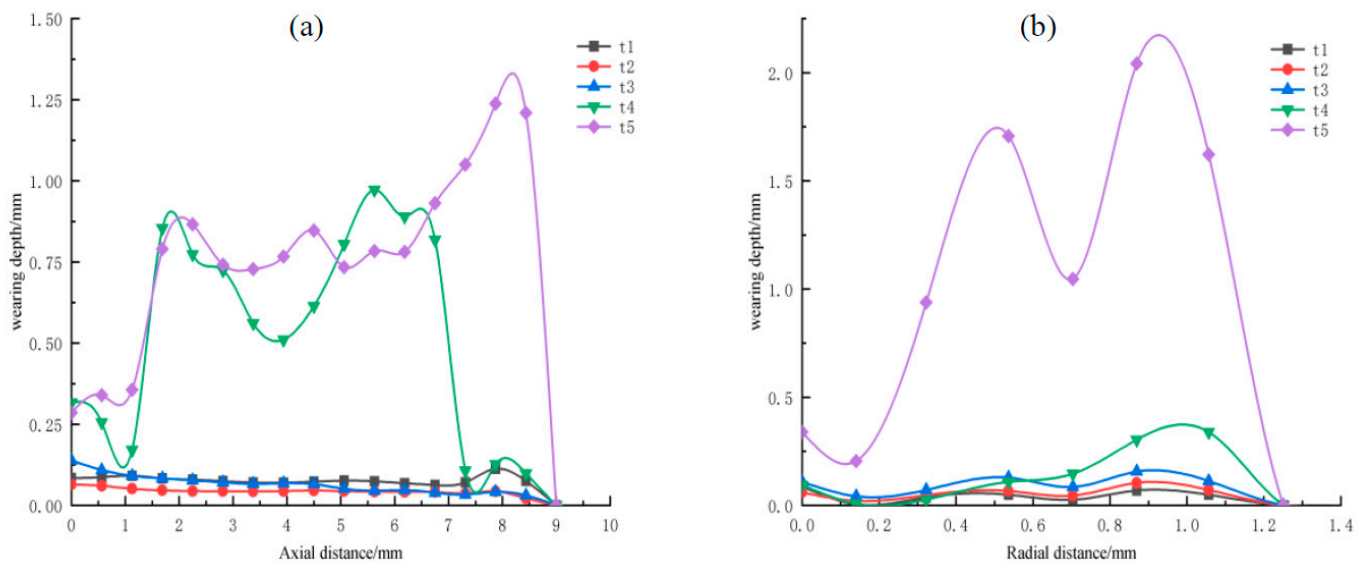


Figure 5. Wear distribution diagram of the tooth surface of the external spline without carburizing treatment when the floating distance is 0.3 mm. (a) Wear depth distribution curve of the external spline in the axial direction; (b) distribution curve of wear depth of external spline in the radial direction.

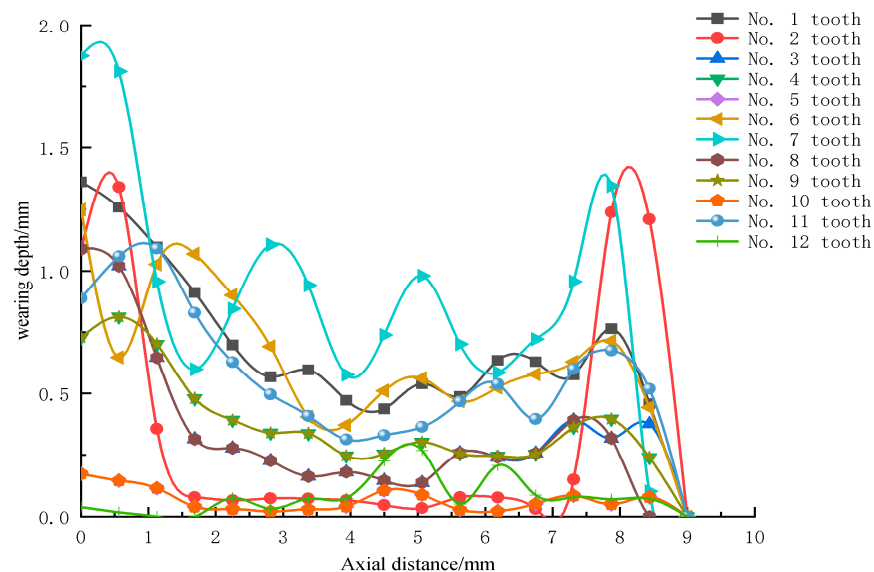


Figure 6. Distribution curve of wear depth on tooth surfaces of external spline without carburizing treatment when floating distance is 0.3 mm.

According to the analysis of Figure 5a,b, the maximum wear depth is at 8 mm along the axial direction, the minimum is at 3 mm to 4 mm, the maximum is at 1.0 mm along the radial direction, and the minimum is from 0 mm to 0.2 mm. Regardless of the axial position or the radial position, the maximum wear depth is located at both ends of the tooth surface, and the middle wear depth is the minimum. The fretting increases with time, resulting in increased wear depth. The fretting wear degree in axial directions t1 and t2 is relatively small, which may be due to the good lubrication effect and the existence of oxide film at the early stage of fretting, so the fretting wear degree is relatively low. The fretting wear degree starts to increase at the t3 and t4 stages in the axial direction, which may be due to the extrusion of lubricating fluid, the rupture of oxide film, and the generation of a large number of metal particles between the contact surfaces of spline couplings. These particles act as abrasive particles after oxidation, which aggravates the fretting wear degree. In the

figure, only the fretting wear degree in the radial direction at the t5 stage is significantly increased, which may be due to the sudden increase in fretting wear degree in the later stage of fretting due to the existence of floating amount.

In Figure 6, it can be found that the wear depth of each tooth is greater due to the increase in floating distance, but the distribution law of wear depth of each tooth still conforms to the fretting wear mechanism of floating aviation involute spline couplings.

4.3. Floating Distance Is 0.6 mm

When the floating distance is 0.6 mm, the actual spline couplings are simulated, and the distribution curve of the axial and radial wear depth of a tooth surface of the involute external spline is obtained, as shown in Figures 7 and 8.

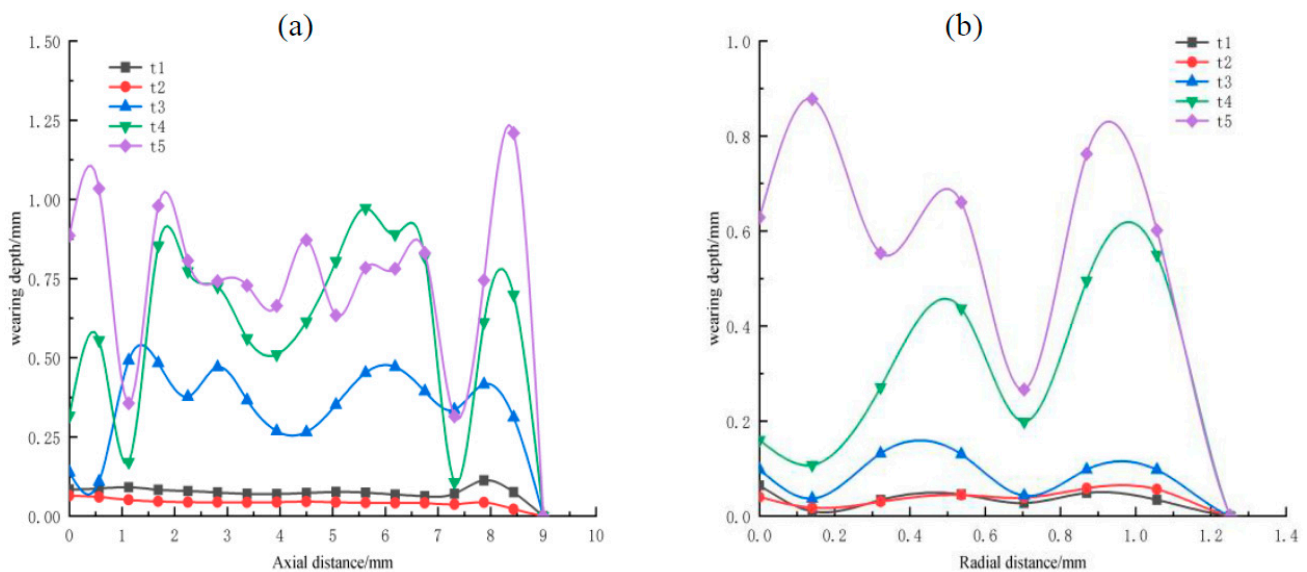


Figure 7. Wear distribution diagram of external spline tooth surface without carburizing treatment when the floating distance is 0.6 mm. (a) Curve diagram of the wear depth distribution of external spline in the axial direction; (b) distribution curve of wear depth of external spline in the radial direction.

According to the analysis of Figure 7a,b, the maximum wear depth is at the position of 0 mm–1 mm and 8 mm–9 mm along the axial direction, the minimum wear depth is at the position of 1 mm and 7 mm, the maximum wear depth is at the position of 0.1 mm and 1 mm along the radial direction, and the minimum wear depth is at the position of 0.7 mm. Regardless of the axial position or the radial position, the maximum wear depth is located at both ends of the tooth surface, and the middle wear depth is the minimum. The fretting increases with time, resulting in increased wear depth. In the figure, the fretting wear degree of axial direction t1 and t2 is relatively small, which is similar to that when the floating distance is 0 mm and 0.3 mm. The fretting wear degree in the axial direction t3, t4, and t5 stages in the figure starts to increase, which may be due to the extrusion of lubricating fluid, the rupture of oxide film, and the generation of a large number of metal particles between the spline couplings contact surfaces. These particles act as abrasive particles after oxidation, which aggravates the fretting wear degree. The fretting wear in the radial direction t3, t4, and t5 stages in the figure increases, which may be due to the sudden increase in fretting wear in the later stage of fretting due to the existence of a floating amount. By comparing Figure 6, it can be found that the wear depth decreases sharply in some areas away from the end of the shaft, which may be caused by the increase in the floating distance. In Figure 8, it can be found that the wear depth on each tooth is greater due to the increase in the floating distance, but the distribution law of the wear

depth of each tooth still conforms to the fretting wear mechanism of the floating aviation involute spline couplings.

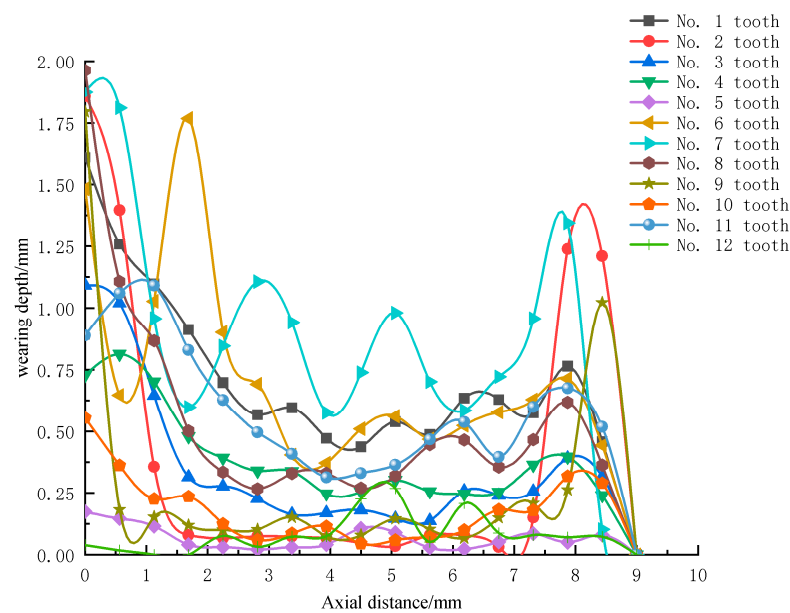


Figure 8. Distribution curve of wear depth on tooth surfaces of external spline without carburizing treatment when floating distance is 0.6 mm.

4.4. Summary

To sum up, through the analysis of the actual working conditions of the floating involute spline couplings, the influence of the floating distance of the spline couplings is considered when calculating the wear depth using the traditional Archard wear formula, and the finite element simulation software is used to carry out the modal simulation of the spline couplings under three floating distance working conditions. The analysis shows that, with the increase in the floating distance, the wear depth of the tooth surface changes significantly, and the wear depth increases along the floating end. The wear distribution of each tooth under the three working conditions is compared and analyzed. The most serious area of tooth surface wear is mainly distributed on both sides of the tooth; with the increase in floating distance, this distribution becomes more significant.

5. Analysis of 32Cr3MoVA Involute Spline Tooth Surface Wear after Carburizing

To conduct the most comprehensive comparative analysis with the 32Cr3MoVA involute spline without carburizing treatment, the performance parameters of the finite element model of the spline couplings are changed to be consistent with the performance parameters of the actual working condition after carburizing treatment and simulated accordingly. This is to further characterize the distribution of the tooth surface in the three wear stages. To further characterize the distribution of the tooth surface in the three wear stages, t_1 is selected from stage I of the wear cycle; t_2 , t_3 , and t_4 are selected from stage II of the wear cycle; and t_5 is selected from stage III of the wear cycle. The wear distribution law of the tooth surface at these five times was analyzed. The distribution curve of the axial and radial wear depth of the tooth surface of the involute spline (external spline as an example) was obtained, as shown in Figures 9–14 (the simulation is only conducted once for each working condition, and the simulation process is unique, so the wear depth value is also non-repeatable.).

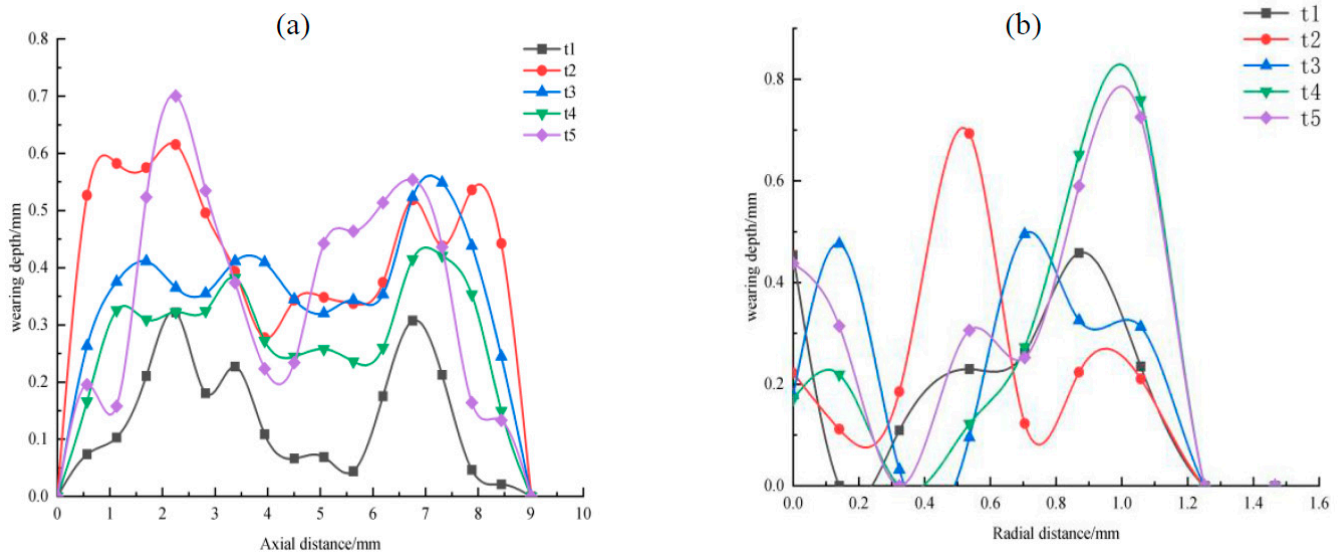


Figure 9. Wear distribution diagram of external spline tooth surface after carburizing when floating distance is 0 mm. (a) Wear depth distribution curve of external spline in the axial direction; (b) distribution curve of wear depth of external spline in the radial direction.

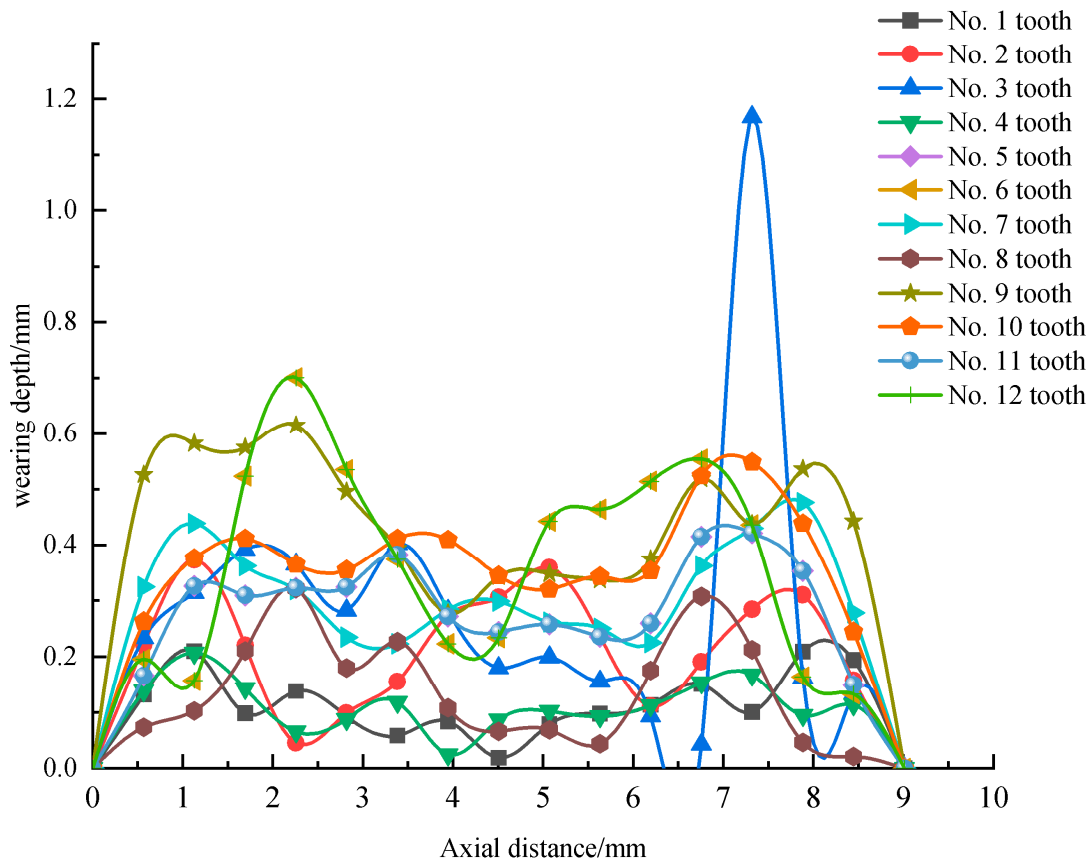


Figure 10. Distribution curve of wear depth of each tooth surface of external spline after carburizing when the floating distance is 0 mm.

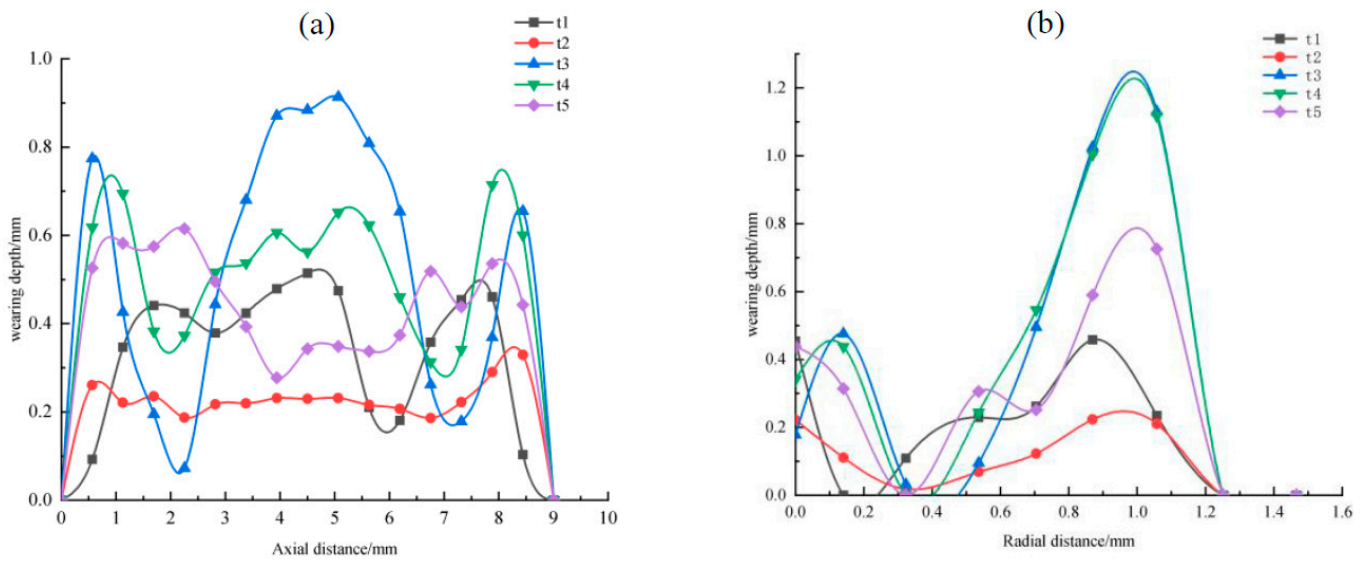


Figure 11. Wear distribution diagram of external spline tooth surface after carburizing when the floating distance is 0.3 mm. (a) Curve diagram of the wear depth distribution of external spline in an axial direction; (b) distribution curve of wear depth of external spline in the radial direction.

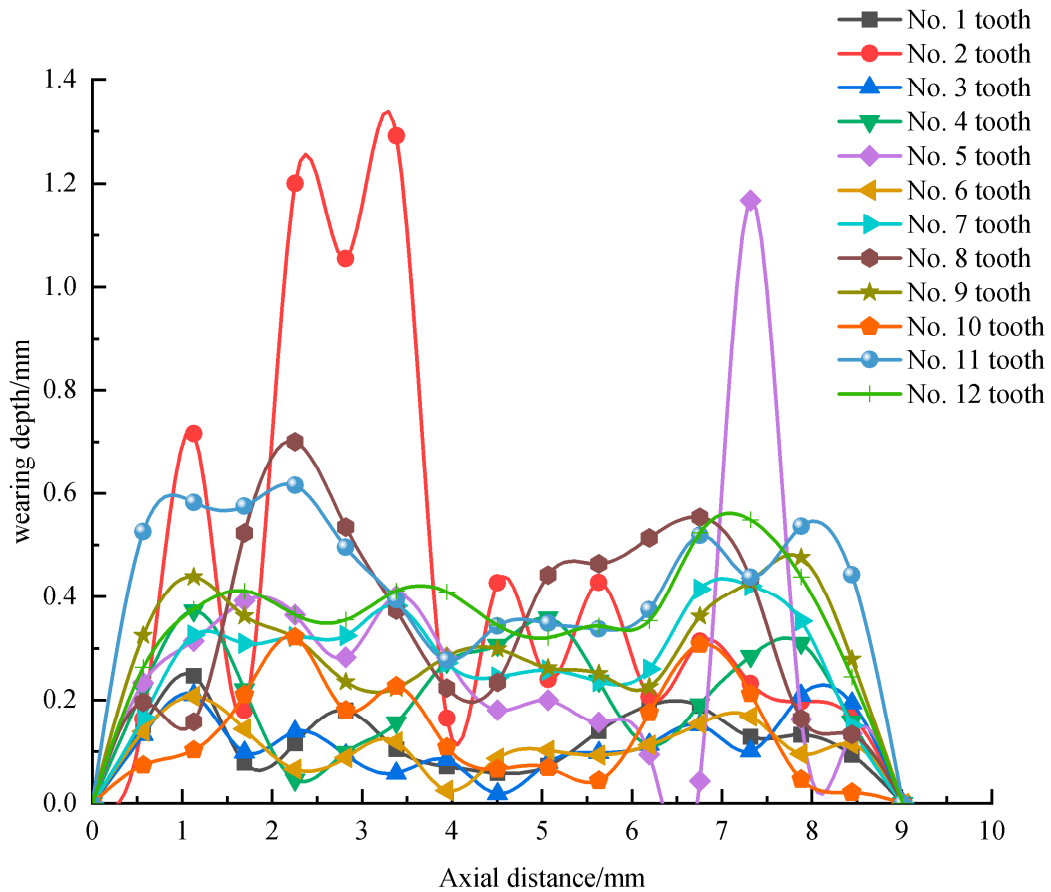


Figure 12. Distribution curve of wear depth of each tooth surface of the external spline after carburizing when the floating distance is 0.3 mm.

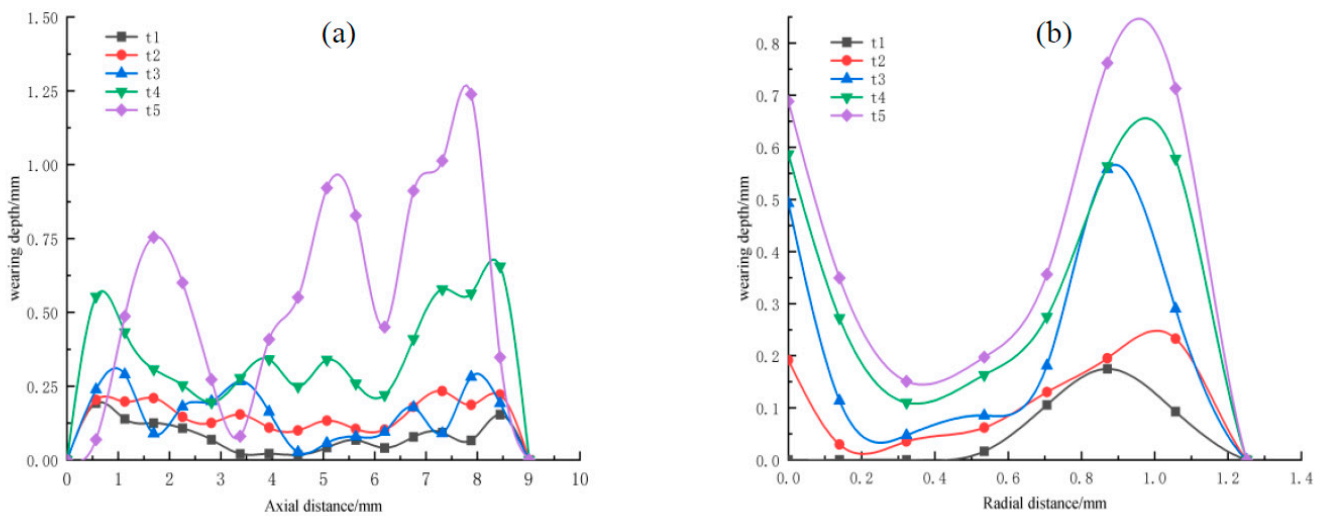


Figure 13. Wear distribution diagram of external spline tooth surface after carburizing when the floating distance is 0.6 mm. (a) Wear depth distribution curve of external spline in the axial direction; (b) distribution curve of wear depth of external spline in a radial direction.

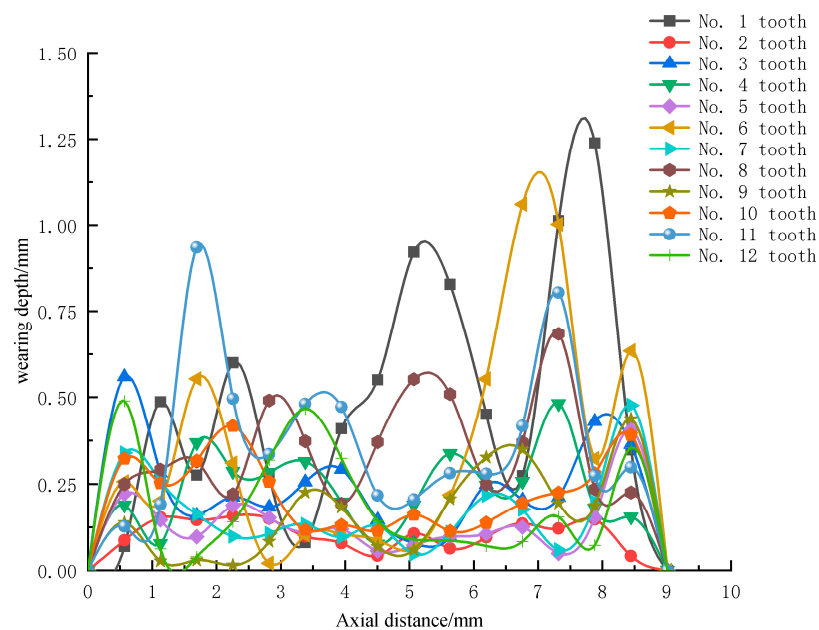


Figure 14. Distribution curve of wear depth of each tooth surface of the external spline after carburizing when the floating distance is 0.6 mm.

5.1. Floating Distance 0 mm

According to Figure 9a,b, the maximum wear depth is at 2 mm along the axial direction, the minimum wear depth is at 4 mm to 7 mm, the maximum wear depth is at 1.0 mm–1.2 mm along the radial direction, and the minimum wear depth is at 0.3 mm. The distribution of wear depth is uniform in both axial and radial positions; In the figure, the fretting wear degree at the t1, t2, t3, and t4 stages is greater than that before carburizing treatment. This may be due to the increased hardness of the tooth surface and a large number of metal particles are produced between the spline couplings’ contact surfaces. These particles act as abrasive particles after oxidation, which aggravates the fretting wear degree. In Figure 10, the wear depth of each tooth is different, which may be caused by tooth clearance and mass eccentricity. However, compared with Figure 10, the wear depth of each tooth has a significant decreasing trend. The wear amount of three teeth is higher at 7 mm–8 mm, which is caused by manual setting error in simulation. However, the wear

depth distribution of other teeth still conforms to the fretting wear mechanism of floating aviation involute spline couplings.

5.2. Floating Distance 0.3 mm

According to Figure 11a,b, the maximum wear depth is at 5 mm along the axial direction, the minimum is at 2 mm and 7 mm, the maximum is at 0.9 mm to 1.0 mm along the radial direction, and the minimum is at 0.3 mm to 0.4 mm. Compared with Figure 5a,b, the axial and radial wear depth slightly increases, which may be caused by the increase in floating distance and the vibration between spline couplings. As shown in Figure 11a, the fretting wear of t1, t2, t3, t4, and t5 stages is relatively high, which may be due to the increased hardness of the tooth surface, and a large number of metal particles are produced between the spline couplings contact surfaces. These particles act as wear particles after oxidation, which aggravates the fretting wear. In Figure 11b, the fretting wear degree in the radial direction is divided into two parts. The wear degree at 0 to 0.6 mm is small, and the wear depth at 0.6 to 1.2 mm is large. This may be due to the sudden increase in fretting wear degree at the later stage of fretting due to the existence of a floating amount.

In Figure 12, as the floating distance increases, the wear depth of each tooth is greater. The wear amount of gear 2 is higher at 1.5 mm–4 mm, and that of gear 5 is higher at 7 mm–8 mm, which is the same as the higher position in Figure 10. This may be due to unskilled grid division and higher wear value caused by manual error. However, the distribution law of the wear depth of each tooth still conforms to the fretting wear mechanism of floating aviation involute spline couplings.

5.3. Floating Distance Is 0.6 mm

In Figure 13, the maximum wear depth is at 7.5 mm along the axial direction, the minimum wear depth is at 3 mm and 3.5 mm, the maximum wear depth is at 0.9 mm to 1.1 mm along the radial direction, and the minimum wear depth is at 0.2 mm to 0.6 mm. Compared with Figure 12, the axial and radial wear depth slightly increases, which may be caused by the increase in floating distance and the vibration of spline couplings. In Figure 13a, t1, t2, and t3 are slightly worn; however, the fretting wear degree in t4 and t5 is relatively high, which may be due to the increased hardness of the tooth surface, and a large number of metal particles are produced between the spline couplings contact surfaces. These particles act as abrasive particles after oxidation, which aggravates the fretting wear degree. In Figure 13b, the fretting wear degree in the radial direction is divided into two parts. The wear degree at 0 to 0.6 mm is small, and the wear depth at 0.6 to 1.2 mm is large. This may be due to the sudden increase in fretting wear degree at the later stage of fretting due to the existence of a floating amount.

Through the analysis of Figure 14, as the floating distance increases, the wear depth of each tooth is greater, but the distribution law of the wear depth of each tooth still conforms to the fretting wear mechanism of floating aviation involute spline couplings.

5.4. Summary

To sum up, through the analysis of the actual working conditions of the floating involute spline couplings for aviation, based on the energy dissipation method, while considering the influence of the floating distance of the spline couplings, the finite element simulation software is used to carry out the modal simulation of the carburized involute spline couplings under three floating distance working conditions, and the analysis shows that the overall trend of the wear degree of the hardened tooth surface becomes smaller; however, with the increase in the floating distance, the wear depth of the tooth surface changes significantly, and the wear depth increases along the floating end.

6. Test

6.1. Test Principle and Device

The test spline couplings are installed on the test bench, and the motor and brake provide stable speed and load. On the test bench, the axial floating distance of the spline shaft can be set, and the misalignment of the shaft can be adjusted to simulate the actual working conditions. The test principle is shown in Figure 15. After a certain period of stable operation of the test platform, the test piece is taken down, the wear of each tooth surface of the spline couplings is observed, and the wear depth of the tooth surface is measured. The analysis results are shown in Section 6.3.

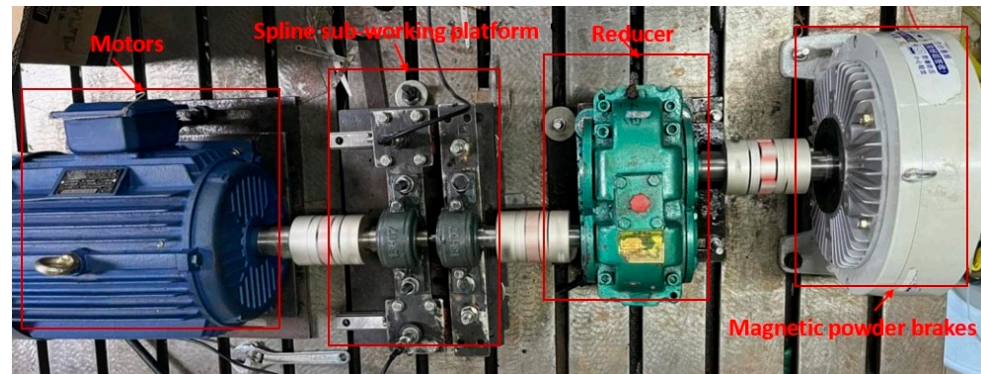


Figure 15. Schematic diagram of test.

This test platform is based on the application environment of the actual aviation floating involute spline couplings. The test platform is made according to the national standard for mechanical design. For each test equipment, the corresponding base is processed. In addition to the installation with the standard T-shaped test platform, it is more important to maintain the axiality of each part of the test platform and avoid the impact of the misalignment of the spline couplings axis on the test results.

During the test, the power train of the whole system is provided by the motor. To ensure accurate control of the motor speed and torque of the transmission system, a vector frequency converter is used to control the motor speed, and the speed is indirectly controlled by changing the frequency. The core of the system load is the magnetic powder brake. The torque of the magnetic powder brake is changed by controlling the input current. The specific model and parameters of the test platform in Figure 15 are shown in Table 4.

Table 4. Model and parameters of test platform equipment.

Equipment Name	Model	Parameter
Three-phase asynchronous motor	YE2-132M-41280	Rated power 7.5 Kw, maximum speed 1500 r/min
Vector frequency converter	ZK880	Power 7.5 Kw, frequency 0–600 Hz
retarder	ZDY-80	Maximum current 2 A, torque 200 Nm
Magnetic powder brake	FZ-200J/Y	Reduction ratio 2.8

6.2. Test Piece Parameters

The correct geometric parameters of involute spline couplings are the basis of the aerospace manufacturing industry, ensuring high precision, high performance, and high reliability. According to the national design standards, the geometric parameters of the spline couplings obtained by design are shown in Table 5 below, and the fit tolerance grade of the internal and external spline couplings is IT6 (all tolerances refer to ANSI B92.1-96). The internal and external spline shafts are shown in Figures 16 and 17.

Table 5. Geometric parameters of spline couplings.

Name	Parameter
Number of teeth z	12
Modulus m	1.25
Pressure angle α ($^\circ$)	30
Spline countershaft diameter D (mm)	30
Fitted length l (mm)	10

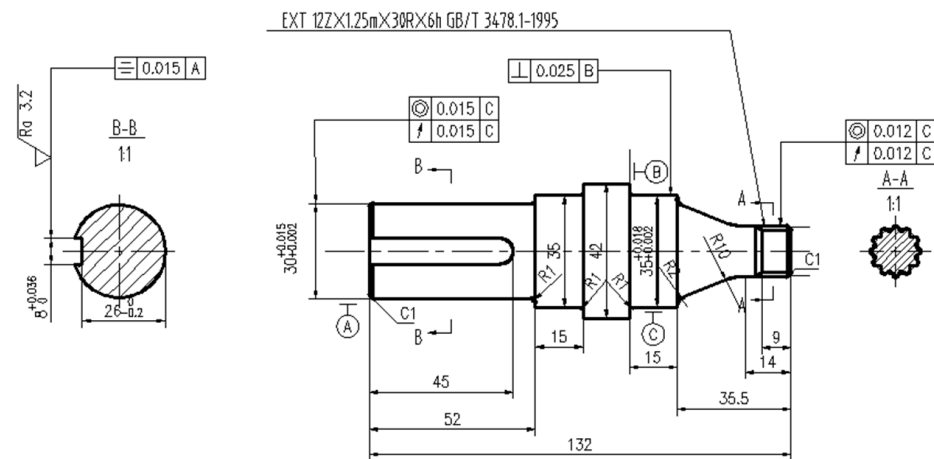


Figure 16. External spline shaft.

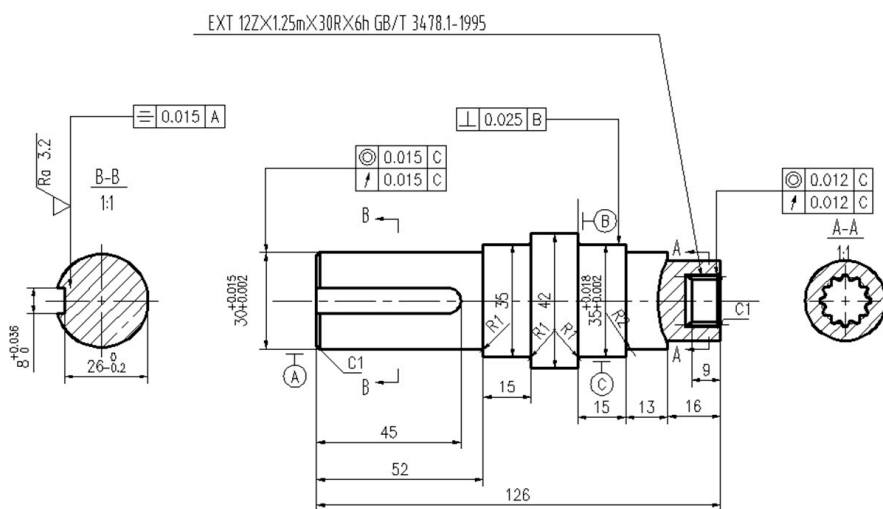


Figure 17. Internal spline shaft.

The test piece materials are shown in the following table. The floating involute spline couplings involved in this paper are made of 32Cr3MoVA alloy steel. Its chemical composition (w-t%) before and after carburizing is shown in Table 6, and its mechanical properties are shown in Table 7. The row corresponding to 1 in the table indicates no carburizing treatment, and the row corresponding to 2 indicates after carburizing treatment.

Table 6. Chemical composition of alloy steel 32Cr3MoVA (wt%).

Item	C	Si	Mn	Mo	Cr	Ni	Fe
1	0.3						
2	0.5	0.25	0.35	0.5	0.7	1.45	Remainder

Table 7. Mechanical properties of 32Cr3MoVA alloy steel.

Mechanical Property	Compressive Strength/MPa	Yield Strength/MPa	Hardness
1	880–980	835–870	269–307 HBS
2	1080–1280	>880	384–433 HBS

6.3. Analysis of Test Results

6.3.1. Macro Analysis of Tooth Surface Topography

To facilitate comparison and analysis, the non-worn tooth surface was observed and a control group was set up. The non-worn tooth surface is shown in Figure 18 below.

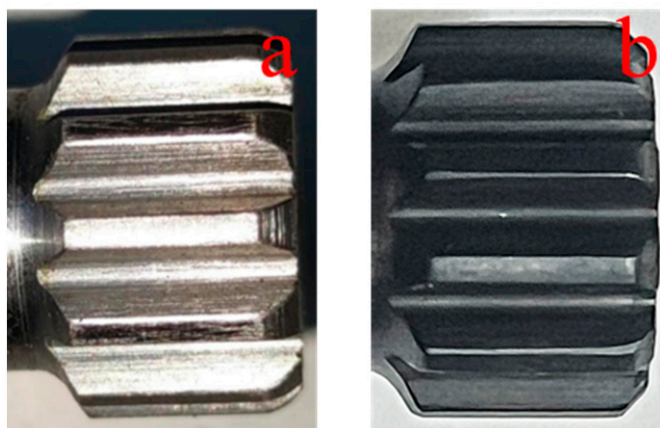


Figure 18. Tooth surface of external spline without wear. (a) External spline without carburizing treatment; (b) external spline with carburizing treatment.

As shown in Figure 18, it is the external spline tooth surface that has not been worn. The wear of the spline tooth surface is investigated by comparing it before and after wear, and the wear of the spline couplings tooth surface under different control groups is analyzed.

Figure 19 shows the wear of some tooth surfaces of the external spline without carburizing treatment under different working conditions. Among them, Figure 19a shows the wear of the tooth surface with an axial floating distance of 0 mm. The wear of the whole tooth surface is relatively serious. It can be seen that many grooves are distributed on the tooth surface, which is caused by repeated friction of wear debris adhering to the tooth surface during the wear process. Figure 19b shows the wear of the tooth surface with an axial floating distance of 0.3 mm, which is more serious than that with a floating distance of 0 mm. With the increase in the floating distance, the wear degree of the tooth surface has changed seriously. The wear distribution difference of the tooth surface is more and more obvious. The left end of the tooth surface is severely worn, while the right end is almost not worn.

By comparing the wear of the spline tooth surface under the three floating distances of Figure 19a,b, as the floating distance increases from 0 mm to 0.3 mm, the wear of the tooth surface is significantly increased, and when the floating distance is 0.3 mm, there are huge block pits on the tooth surface, that is, the tooth surface is severely deformed.

As shown in Figure 20, the wear of some tooth surfaces of the external spline under different working conditions after carburizing treatment. Figure 20a shows the wear of the tooth surface with an axial floating distance of 0 mm. There are many dotted pits on the tooth surface, and it can be seen that the edge positions at both ends of the key teeth are relatively worn. Figure 20b shows the wear of the tooth surface with an axial floating distance of 0.3 mm; the wear of the tooth surface is severe, and the pits on the tooth surface are densely distributed.

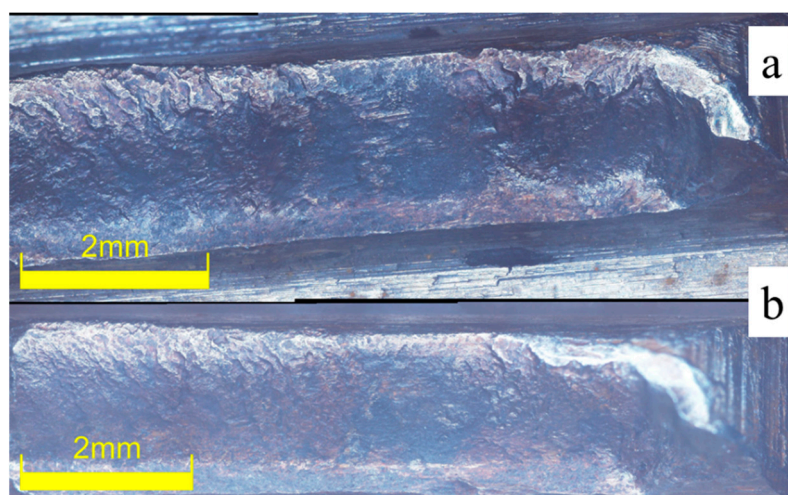


Figure 19. Typical tooth surface wear of splines without carburizing. (a) Wear of external splines with a floating distance of 0 mm; (b) wear of external spline tooth surface when the floating distance is 0.3 mm.

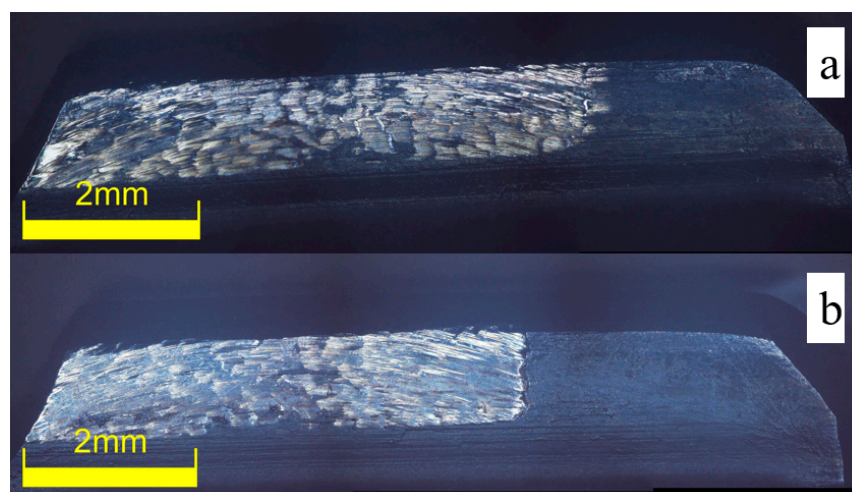


Figure 20. Typical tooth surface wear of spline after carburizing. (a) External spline tooth surface wear when floating distance is 0 mm; (b) wear of external spline tooth surface when the floating distance is 0.3 mm.

6.3.2. Microanalysis of Tooth Surface Topography

To observe the wear of the external spline in the test process more clearly, the wear mechanism of the floating involute spline couplings is analyzed. Typical worn tooth surfaces under various working conditions were selected for local magnification, as shown in Figures 21 and 22 (Figure 21 shows the tooth surface without carburizing treatment; Figure 22 shows the tooth surface after carburizing treatment).

In Figure 21a, when the axial floating distance is 0 mm, many small pits formed by wear can be seen, and the pits formed by large pieces of material being worn off. It was found that the wear mechanism of the spline tooth surface is mainly abrasive wear. There are also many grooves on the tooth surface, which is caused by the repeated movement of abrasive particles on the tooth surface during the wear process. The main form of wear here is adhesive wear. In Figure 21b, when the axial floating distance is 0.3 mm, it can be seen that the adherent abrasive particles are more densely distributed. In addition, cracks of different sizes are distributed on the tooth surface. This is because with the increase in the floating distance, the stability of the system decreases, the force is uneven, and the grooves on the tooth surface develop into cracks. When the float increases, a slope-like

wear scar will appear on the uneven surface. At this time, there are also adhesive wear and abrasive wear. At the same time, it can be seen in Figure 21 that the tooth surface is slightly red. This is because, during the experiment, the contact tooth surface is mixed with oxygen, and oxidation wear occurs.

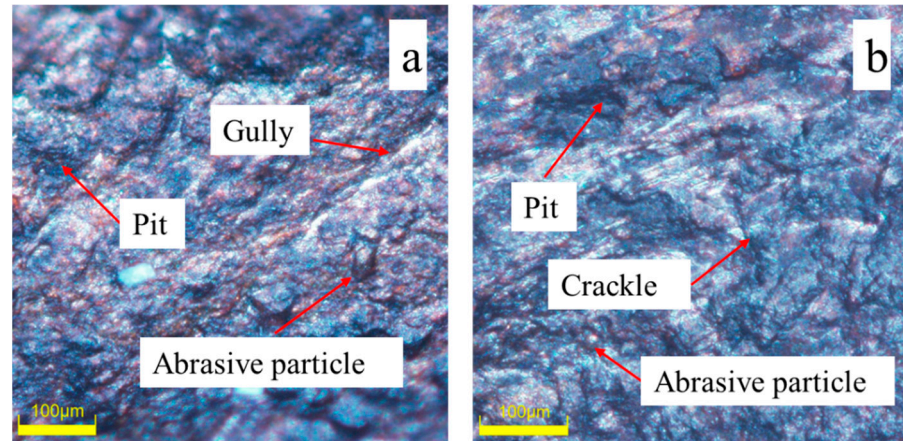


Figure 21. Partial enlargement of typical tooth surface wear of spline without carburizing treatment. (a) Wear of external spline tooth surface when floating distance is 0 mm; (b) wear of external spline tooth surface when the floating distance is 0.3 mm.

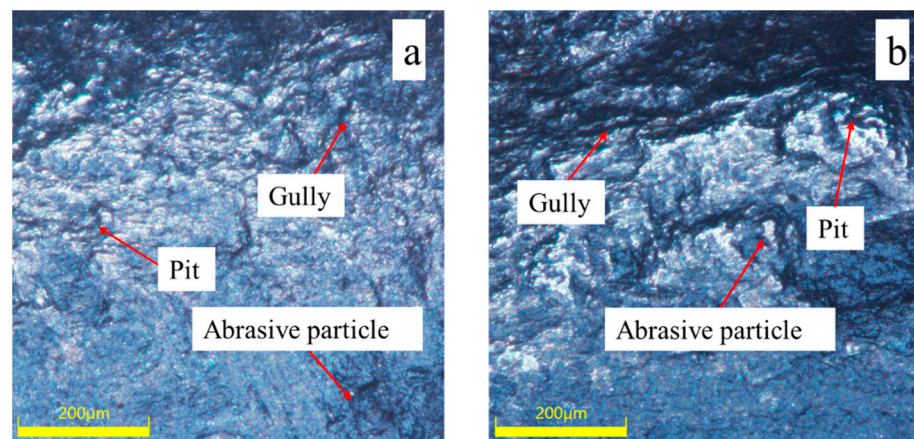


Figure 22. Local enlargement of typical tooth wear of spline after carburizing. (a) External spline tooth surface wear when floating distance is 0 mm; (b) wear of external spline tooth surface when the floating distance is 0.3 mm.

Figure 22 shows the wear of some tooth surfaces of the external spline under different working conditions after carburizing treatment. In Figure 22a, we can see densely distributed small pits, pits formed by wear, and gullies of different sizes. It is analyzed that the wear mechanism of spline tooth surface here is mainly abrasive wear and adhesive wear. Dense pits and crisscross gullies can be seen in Figure 22b, which is caused by the increase in floating distance, the worse meshing state of spline couplings, and the greater friction between teeth. For the spline pair that has been carburized, with the increase in floating distance, the wear degree of the tooth surface is still increased, but compared with the spline that has not been carburized, the wear degree of the tooth surface is reduced.

6.3.3. Analysis of Tooth Surface Wear Depth

To analyze the difference between the theoretical simulation results and the experimental wear, the wear depth of the tooth surface is now counted when the floating distance before and after carburizing treatment is 0 mm and 0.3 mm. An Olympus digital microscope (as shown in Figure 23) is used to observe the tooth surface, and the tooth top,

middle and root of the tooth surface under various working conditions are measured (as shown in Figure 24). The height difference between the worn part and the non-worn part is measured, each tooth is measured three times, and the average value is taken as the final wear depth value.

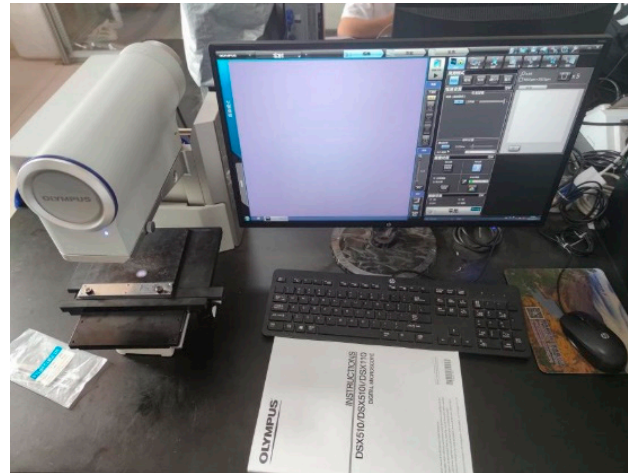


Figure 23. Olympus DSX510 digital microscope.

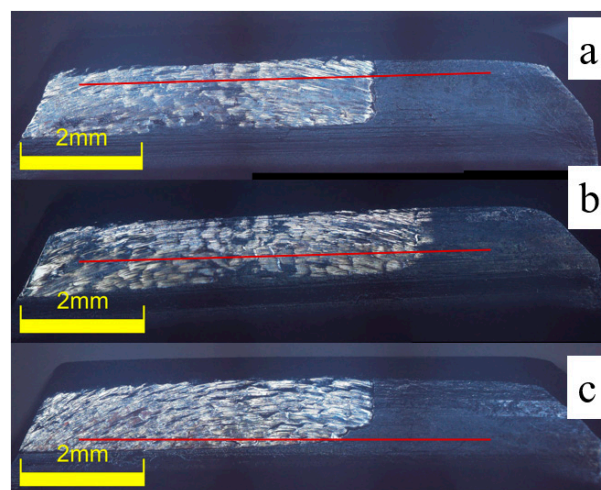


Figure 24. Measuring the wear depth of tooth surface. (a) Top position of tooth surface; (b) middle position of tooth surface; (c) root position of tooth surface.

Finally, the theoretical wear depth curves and actual wear depth curves under various working conditions are obtained, as shown in Figures 25 and 26.

When the floating distance is 0 mm, as shown in Figure 25, the wear of each tooth surface of the involute spline without carburizing treatment is relatively large. It can be seen that the wear depth of 1, 2, and 3 teeth are larger; this may be caused by manual installation and unloading of spline couplings. Whether before or after carburizing treatment, the general trend of wear depth of each tooth is that the test measured value is slightly larger than the simulation value, which is caused by the installation error of the test bench.

When the floating distance is 0.3 mm, as shown in Figure 26, it is obvious that the wear depth of each tooth surface increases with the increase in the floating distance. It can be seen that the wear depth of 3 and 10 teeth is larger and that of 12 teeth is smaller; this is due to the existence of the floating distance, which leads to the increase in the vibration amplitude of the spline in the working process and uneven stress. However, the distribution law of the wear depth of each tooth still conforms to the fretting wear mechanism of the floating aviation involute spline couplings.

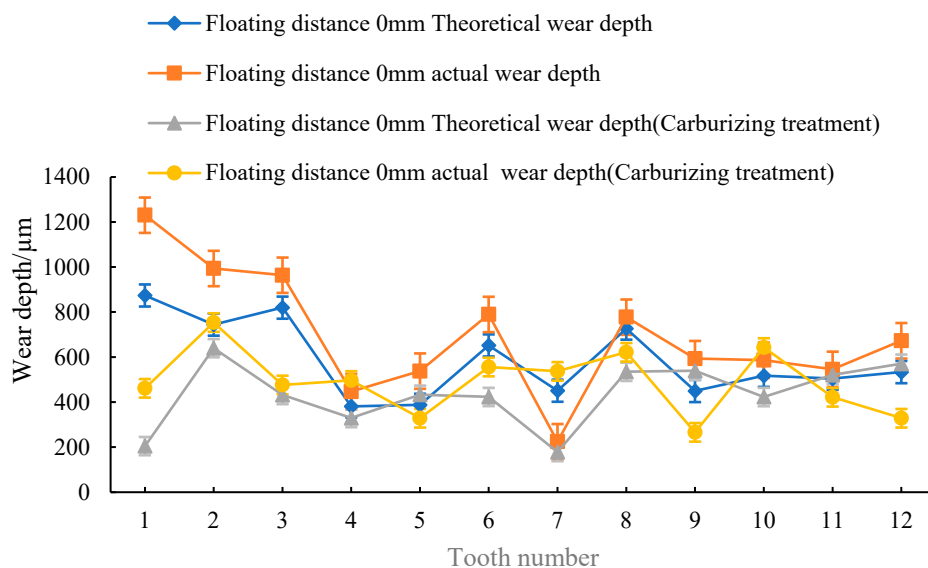


Figure 25. Comparison of theoretical and actual values of wear depth of each tooth of involute spline before and after carburizing when the floating distance is 0 mm.

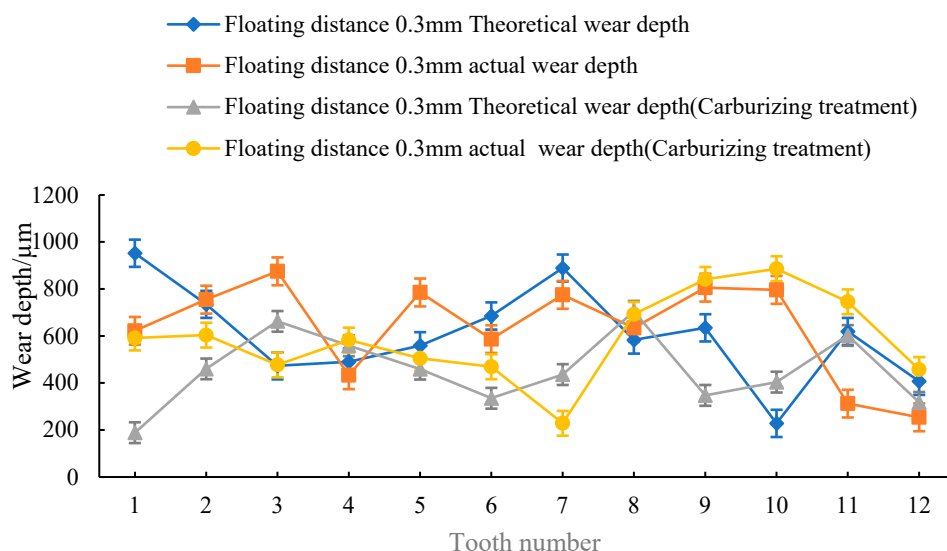


Figure 26. Comparison of theoretical and actual values of wear depth of each tooth of involute spline before and after carburizing when the floating distance is 0.3 mm.

6.4. Summary

Through the floating involute spline test bench, various working conditions in Sections 3 and 4 are tested and verified. The conclusions are as follows: with the increase in floating distance, the wear depth of spline teeth continues to increase whether before or after hardening treatment; in addition, the test value is slightly larger than the theoretical value, which is caused by the installation error of the test bench. To make the theoretical value closer to the actual value, it is necessary to improve the accuracy of the test bench.

7. Conclusions

In this work, based on the energy dissipation method, a wear prediction model suitable for the aviation floating involute spline couplings is proposed, and the wear distribution of the aviation floating involute spline couplings before and after carburizing is simulated and analyzed. Finally, the simulation results under the prediction model are verified by experiments. The conclusions are as follows:

(1) Through Abaqus simulation analysis, whether the tooth surface is carburized or not, the wear depth of each tooth of the involute spline couplings will increase with the increase in the floating distance. When the floating distance is 0.3 mm, the wear depth of the tooth surface changes significantly, and the wear depth increases along the floating end, which aggravates the wear of the spline couplings. When the wear depth reaches a certain value, the spline couplings are severely deformed, which cannot meet the use requirements.

(2) Since the fact that the aviation floating involute spline couplings has axial runout, the axial runout speed is coupled with the relative slip rate caused by the contact between teeth, and the wear calculation model applicable to the aviation floating involute spline couplings is reliable.

(3) The most serious wear area of the floating spline couplings is mainly distributed at the edge of the tooth. With the increase in floating distance, this distribution becomes more significant.

(4) When the floating distance is small, by comparing the wear of each tooth surface before and after carburizing treatment, it can be seen that carburizing treatment can improve the performance of the tooth surface, reduce the wear of the tooth surface, and increase the service life of the spline; when the floating distance is too large, the performance of the spline couplings is less affected by carburizing treatment.

Author Contributions: Methodology, X.X.; Validation, J.L., Y.L. and J.J.; Resources, S.Y.; data curation, J.L., Y.L. and J.J.; Writing—original draft preparation, J.L. All authors have read and agreed to the published version of the manuscript.

Funding: The authors acknowledge financial support from the National Natural Science Foundation (Grant No. 52005312) and supported by Sichuan Science and Technology Program (2023YFG0201).

Data Availability Statement: The data presented in this study are available on request from corresponding author or the second.

Conflicts of Interest: The authors declare that there are no conflicts of interest regarding the publication of this article.

References

1. Xiao, L.; Xu, Y.; Chen, Z.; Sun, X.; Xu, H. Prediction of fretting damage and wear fatigue of floating involute splines. *J. Northwest Polytech. Univ.* **2022**, *40*, 549–559. [[CrossRef](#)]
2. Curà, F.; Mura, A. Theoretical and numerical evaluation of tilting moment in crowned teeth splined couplings. *Meccanica* **2018**, *53*, 413–424. [[CrossRef](#)]
3. Xue, X.Z.; Wang, S.M. Dynamic Characteristics and Load Coefficient Analysis of Involute Spline Couplings. *Adv. Mater. Res.* **2014**, *890*, 450–454. [[CrossRef](#)]
4. Xue, S.; Wang, M.; Yuan, R. *Investigation of Load Distribution among Teeth of An Aero-Engine Spline Coupling*; Springer: Berlin/Heidelberg, Germany, 2016; Volume 367, pp. 1152–1162.
5. Tang, Y.; Meng, J.; Xia, F. Analysis of the influence of lubrication and surface treatment on the wear of the spline couplings of the helicopter reducer. *Mech. Res. Appl.* **2021**, *34*, 60–62.
6. Xu, Y. *Strength and Wear Analysis of Involute Spline of Aircraft Flap Transmission System*; Chongqing University: Chongqing, China, 2018.
7. Yu, Y.; Hu, Y.; Dai, X.; He, Z.; Li, M. Fretting wear analysis and parameter optimization of spline couplings. *Mech. Sci. Technol.* **2021**, *40*, 828–834.
8. Tan, Y.; Jiang, L.; Jiang, S.; Yang, S.; Liu, S.; Hu, Q. Analysis of fretting friction contact of involute spline couplings. *J. Mech. Eng.* **2018**, *54*, 123–130. [[CrossRef](#)]
9. Jiang, L. *Research on Fretting Wear of Floating Involute Spline Couplings*; Xiangtan University: Xiangtan, China, 2018.
10. Wei, Y.; Liu, L. Load distribution and stress analysis of tooth direction and tooth profile of shield spline connection. *Eng. Mach.* **2017**, *48*, 10–15.
11. Wei, Y.; Liu, L.; Xiao, R.; Li, J. Research on tooth modification of shield spline shaft. *Mech. Manuf.* **2018**, *56*, 90–93.
12. Ratsimba, C.H.H.; McColl, I.R.; Williams, E.J.; Soh, H.P. Measurement, analysis and prediction of fretting wear damage in a representative aeroengine spline coupling. *Wear* **2004**, *257*, 1193–1206. [[CrossRef](#)]
13. Hyde, T.R.; Leen, S.B.; McColl, I.R. A simplified fretting test methodology for complex shaft couplings. *Fatigue Fract. Eng. Mater. Struct.* **2005**, *28*, 1047–1067. [[CrossRef](#)]
14. Baker, D.A. A Finite Element Study of Stresses in Stepped Splined Shafts, and Partially Splined Shafts Under Bending, Torsion, and Combined Loadings. *Va. Tech.* **1999**, *6*, 41–47.

15. Leen, S.B.; Richardson, I.J.; McColl, I.R.; Williams, E.J.; Hyde, T.R. Macroscopic fretting variables in a splined coupling under combined torque and axial load. *J. Strain Anal. Eng. Des.* **2001**, *36*, 481–497. [[CrossRef](#)]
16. Leen, S.B.; Hyde, T.H.; Ratsimba, C.; Williams, E.J.; McColl, I.R. An investigation of the fatigue and fretting performance of a representative aero-engine spline coupling. *J. Strain Anal. Eng. Des.* **2002**, *37*, 565–583. [[CrossRef](#)]
17. Madge, J.J.; Leen, S.B.; Shipway, P.H. A combined wear and crack nucleation propagation methodology for fretting fatigue prediction. *Int. J. Fatigue* **2008**, *30*, 1509–1528. [[CrossRef](#)]
18. Olver, A.V.; Medina, S. Tribology of spline couplings. *Tribol. Ser.* **2003**, *41*, 589–602.
19. Medina, S.; Olver, A.V. Regimes of contact in spline couplings. *Trans. Am. Soc. Mech. Eng. J. Tribol.* **2002**, *124*, 351–357. [[CrossRef](#)]
20. Medina, S.; Olver, A.V. An analysis of misaligned spline couplings. *J. Eng. Tribol.* **2002**, *216*, 269–279. [[CrossRef](#)]
21. Hong, J.; Talbot, D.; Kahraman, A. A semi-analytical load distribution model for si-de fit involute splines. *Mech. Mach. Theory* **2014**, *76*, 39–55. [[CrossRef](#)]
22. Hong, J.; Talbot, D.; Kahraman, A. Load distribution analysis of clearance fit spline joints using finite elements. *Mech. Mach. Theory* **2014**, *74*, 42–57. [[CrossRef](#)]
23. Ding, J.; Mccoll, I.; Leen, S. The application of fretting wear modelling to a spline coupling. *Wear* **2007**, *262*, 1205–1216. [[CrossRef](#)]
24. Ding, J.; Madge, J.; Leen, S.B.; Williams, E.J. Towards the modelling of fretting wear and fatigue interaction in spline couplings. *Appl. Mech. Mater.* **2006**, *5*, 165–172. [[CrossRef](#)]
25. Hattori, T.; Watanabe, T. Fretting fatigue strength estimation considering the fretting wear process. *Tribol. Int.* **2006**, *39*, 1100–1105. [[CrossRef](#)]
26. Matveevsky, R.M. The critical temperature of oil with point and line contact machines. *Trans. ASME* **1965**, *87*, 754. [[CrossRef](#)]
27. Sauger, E.; Fouvry, S.; Ponsonnet, L.; Kapsa, P.; Martin, J.M.; Vincent, L. Tribologically transformed structure in fretting. *Wear* **2000**, *245*, 39–52. [[CrossRef](#)]
28. Fouvry, S.; Kapsa, P.; Vincent, L. An elastic–plastic shakedown analysis of fretting wear. *Wear* **2001**, *247*, 41–54. [[CrossRef](#)]
29. Zhang, T.; McHugh, P.E.; Leen, S.B. Computational study on the effect of contact geometry on fretting behaviour. *Wear* **2011**, *271*, 1462–1480. [[CrossRef](#)]
30. Zhang, M.; Pang, D.; Wang, H.; Huang, T.; Ming, M. Energy dissipation characteristics of linear normal vibration contact interface. *Mech. Strength* **2022**, *44*, 788–794.
31. Yang, W.; Guo, X.; Zhao, Y. Effect of convection and radiation heat transfer on estimation of metal high cycle fatigue energy dissipation. *J. Mech. Eng.* **2021**, *57*, 187–195.
32. Zheng, W.; Wang, S.; Jie, X.; Li, H. Energy dissipation method for fretting wear analysis of involute spline couplings. *China Mech. Eng.* **2017**, *28*, 2171–2176.
33. Xue, X. *Research on Fretting Wear Mechanism and Wear Prediction Method of Aviation Involute Spline Couplings*; Northwest Polytechnical University: Xi'an, China, 2017.

Disclaimer/Publisher's Note: The statements, opinions and data contained in all publications are solely those of the individual author(s) and contributor(s) and not of MDPI and/or the editor(s). MDPI and/or the editor(s) disclaim responsibility for any injury to people or property resulting from any ideas, methods, instructions or products referred to in the content.